Manuscript prepared for The Cryosphere
with version 2015/11/06 7.99 Copernicus papers of the LaTeX class copernicus.cls.
Date: 20 April 2016

Arctic sea ice diffusion from observed and simulated Lagrangian trajectories

Pierre Rampal[1], Sylvain Bouillon[1], Jon Bergh[1], and Einar Olason[1]

[1]Nansen Environmental and Remote Sensing Center and Bjerknes Centre for Climate Research, Thormøhlens gate 47, 5006 Bergen, Norway

Correspondence to: Pierre Rampal (pierre.rampal@nersc.no)

Abstract. Due to the difficult access, an oil spill occurring in ice-covered regions of the ocean in fall or winter may persist for several months and therefore could affect large areas and impact the local ecosystems. When reaching the surface, the oil accumulates under the ice cover or in leads before being trapped in the new ice formed. Oil spill risk assessment and response planning then need to be based on an accurate description of the long term mean sea ice circulation and the effect of the unpredictable fluctuating part of the sea ice motion. In this study we characterise sea ice drift by applying a Lagrangian diffusion analysis to buoy trajectories from the International Arctic buoy Program (IABP) dataset and from two different models (the standalone Lagrangian sea ice model neXtSIM and the coupled ice-ocean model used for the TOPAZ reanalysis) run on two different configurations. By applying the diffusion analysis to the IABP buoy trajectories over the period 1979-2011, we confirm that sea ice diffusion follows two distinct regimes ("ballistic" and "Brownian") and we provide accurate values for the diffusivity and integral time scale that could be used in Eulerian or Lagrangian passive tracers models to simulate the transport and diffusion of particles moving with the ice. We discuss how these values are linked to the evolution of the fluctuating displacements variance and how this information could be used to define the size of the searching area around the position predicted by the mean drift. By comparing observed and simulated sea ice trajectories for three consecutive winter seasons (2007-2011), we show how the characteristics of the simulated motion may differ or fit well with observations. This comparison illustrates the utility of using diffusion analysis to evaluate the output of modelling system that includes a sea ice model before using them to simulate the transport of passive tracers in sea ice.

1 Introduction

The increasing activities in the Arctic seas (e.g. shipping, fishing, and oil and gas exploration and exploitation) enhance the risk of pollution in a region where ecosystems are already under threat from the amplified effects of climate change. The extreme conditions (e.g., presence of ice, extreme cold, high winds, and the Polar night) and the long distance from well-equipped facilities may render access to the polluted area difficult or even impossible for long periods of time (even longer than 6 months in winter) (Drozdowski et al., 2011). These conditions also render the detection of the pollution challenging, and slow or even stop the natural and artificial degradation processes. In addition, the pollutants are often trapped in or under the ice and, therefore, may be transported over large distances before being released (Rigor and Colony, 1997). In that context, better understanding the trajectories of sea ice (and then of the passive tracers following it) could be crucial for risk assessment and response planning related to pollutant release in Arctic seas. Note that passive tracer modelling in sea ice has also other applications, for example to study biology and its link with pollutants (e.g. Borgå et al., 2002; Pfirman et al., 1995) or to estimate the age of the Arctic sea ice cover (e.g. Fowler et al., 2004; Hunke, 2014).

Sea ice motion can be viewed as a superposition of a mean circulation and turbulent-like fluctuations (Rampal et al., 2009b). Using such decomposition for studying pollutant transport by sea ice was already proposed by Colony and Thorndike (1985) who analysed sea ice drift data covering the period 1893-1984 while using arbitrary averaging scales (90 years and 1500 km) to define the mean motion. By using a denser sea ice drift dataset covering the period 1978-2001 and the theoretical framework introduced by Taylor (1921) for the analysis of turbulent fluids, Rampal et al. (2009b) proposed a methodology to rigorously decompose sea ice motion into mean and turbulent-like fluctuating parts. The appropriate averaging scales (about 400 km and 5.5 months for winter conditions) were found small enough to clearly separate the inter-annual variability of the mean circulation from the fluctuating motion due to passing atmospheric perturbations, local oceanic eddies and inertial and tidal motion. This approach based on the analysis of single particle trajectories has been widely used to study diffusion properties from Lagrangian drifters in the ocean (see e.g., Zhang et al., 2001; Poulain and Niiler, 1989) and is now becoming a standard analysis tool for sea ice dynamics (Lukovich et al., 2011, 2015).

Single particle analysis (here referred to as diffusion analysis) is particularly useful for characterising long-term trajectories as it clearly decomposes the motion into a mean/predictable and fluctuating/unpredictable parts (Colony and Thorndike, 1985). It also allowed Rampal et al. (2009b) to show that sea ice diffusion exhibits a clear transition from the so-called ballistic regime to the Brownian regime. This transition is also typical of turbulent fluids and is due to the fast decay of the velocities autocorrelation function. The information coming from the diffusion analysis (mean flow and diffusivity) statistically describe the ensemble of all the potential trajectories that a particle,

released at a given location at an unknown time during a season, could follow, and may then be sufficient to produce a probabilistic forecast of tracer transport.

To simulate tracer transport, one can use continuous or discrete passive tracer models. Continuous models are usually based on the following advection-diffusion equation:

$$\frac{\partial C}{\partial t} + \bar{\mathbf{u}} \cdot \nabla C = \nabla \cdot (K \nabla C), \tag{1}$$

where $\bar{\mathbf{u}}$ is the mean velocity field and K is the corresponding diffusivity (LaCasce, 2008). One can also use discrete passive tracer models for which the displacement dx_i in the i direction is defined for independent objects. The simplest approach, known as the "random walk" model or zeroth order model, is strictly equivalent to the advection-diffusion equation of continuous models and simply defines dx_i by

$$dx_i = \bar{u}_i dt + \sqrt{2}\sqrt{\langle u_i'^2 \rangle} dw_i, \tag{2}$$

where u_i' is the fluctuating velocity in the i direction and dw_i is a Weiner process. The first order approach is also often used as it can represent the transition between the ballistic and the Brownian diffusion regimes by applying the stochastic term on the evolution of the velocity, leading to the following set of equations:

$$dx_i = (u_i + \bar{u}_i) dt \tag{3}$$

$$du_i = -\frac{1}{\Gamma_i} u_i dt + \sqrt{\frac{2}{\Gamma_i}} \sqrt{\langle u_i'^2 \rangle} dw_i. \tag{4}$$

where Γ_i is the integral time scale in the i direction. First-order approaches can also successfully reproduce the loops often seen in surface drifter trajectories by adding a rotation term similar to Coriolis term.

These approaches have been widely used to study the spread of pollutant and other tracers by eddy turbulence in the ocean and atmosphere (see LaCasce, 2008, for an extensive review). However, using such approaches to simulate the spread of sea ice would be inappropriate because of the characteristics of sea ice motion fields which are intermittent in time and discontinuous in space. Such approaches may still be used and have been used to reproduce the statistics of individual sea ice trajectories. The "random walk" model was for example used in Colony and Thorndike (1985) with a mean field and statistics on the fluctuations derived by (Colony and Thorndike, 1984). Alternatively the advection-diffusion equation could be used as a stochastic differential equation where C describes the probability for a particle to be in a given position after a given time.

Another way to use passive tracer models is to replace the mean field $\bar{\mathbf{u}}$ in Equations 1, 2 or 3 by simulated/observed Eulerian velocity fields. This approach is widely used with passive tracer models directly forced by motion fields simulated by an hydrodynamical model (e.g. Nudds et al., 2013), given by a reanalysis (e.g. Gearon et al., 2014) or derived from satellite observations (e.g. Fowler et al., 2004). The diffusion term (or in the discrete models, the Wiener process term) is either neglected or defined to account for the unresolved part of the fluctuating motion. The unresolved part

of the motion could be analysed with the methodology proposed by Dominicis et al. (2012) for ocean surface tracer modelling, which consists of comparing the characteristics of the fluctuating part of observed trajectories to the ones of trajectories given by a tracer model forced by model output.

Before using one of these approaches one needs to answer a few questions: What are the right averaging scales to define the mean motion field? What are the statistical properties of the fluctuating part of the motion? Is there a transition between different regimes of diffusion? Are the mean and fluctuating parts of the motion correctly reproduced by the forcing field? If not, could this indicate that some processes are missing in the forcing velocity fields? If the fluctuating part is not well reproduced could it be compensated by adding extra terms in the tracer equation? Those important questions are not always answered before running tracer models forced by sea ice velocity fields and this could strongly impact the validity of the studies based on such results.

In this paper, we demonstrate the interest of applying Lagrangian diffusion analysis on sea ice trajectories in the context of passive tracer modelling. The analyses presented in this paper are restricted to winter conditions, as it has been identified as more critical for oil spill recovery operations. In Section 2, we apply the same method as in Rampal et al. (2009b) to the IABP buoys dataset for the period 1979-2011. This reference dataset is analysed to get an overall picture of the characteristic of the mean and fluctuating part of the motion for the Central Arctic domain and to derive the quantities (diffusivity, Lagrangian integral time scale, etc.) needed for tracer models. This section also includes a discussion on how to predict the evolution of the fluctuating displacements variance, which could be used to define the size of the searching area around the trajectory predicted by the mean drift. In Section 3, we follow the methodology proposed by Dominicis et al. (2012), which consists of applying the diffusion analysis to observed and simulated trajectories to evaluate the merits of using these simulated fields for tracer modelling. This evaluation exercice is done for two different simulations obtained with for two different models run in different configurations. Section 4 sums up the main conclusions.

2 Diffusion analysis on a reference dataset

In this section we present the theoretical framework of the diffusion analysis by showing its application to the IABP dataset from 1979 to 2011 as a reference. Results and theory are then compared and discussed in the context of passive tracer modelling. This is the same analysis as that already done by Rampal et al. (2009b), except that we use the 12-hourly buoy positions data (Rigor, I. G. Compiled by Polar Science Center. 2002. IABP Drifting Buoy Pressure, Temperature, Position, and Interpolated Ice Velocity, Version 1. subset C. Boulder, Colorado USA. NSIDC: National Snow and Ice Data Center. http://dx.doi.org/10.7265/N53X84K7. January 2015) and extend the analysis period up to 2011. The results we obtained are very similar to those reported in Rampal et al. (2009b), but additional evaluation and discussion is presented in subsection 2.4.

2.1 Reference dataset

Figure 1 shows all the trajectories analysed in this section. We restrict the analysis to the winter period defined as starting the 1^{st} of November and ending the 15^{th} of May. Results for summer can be found in Rampal et al. (2009b). To investigate sea ice motion properties in the pack ice, we restricted the IABP dataset to a region located in the centre of the Arctic basin (hereafter denoted the Central Arctic domain). This includes all buoy data north of 70°N, except between 20°W and 100°E where the southern limit is set to 80°N. In addition only buoy data from more than 100 km off the coast is used. The selected data cover the whole Central Arctic basin, but the data coverage in the East Siberian and Laptev Seas is sparse. Sea ice dynamics in coastal regions are specific with for example the presence of land-fast ice and would require a dedicated study. The IABP buoys are mainly deployed over multi-year ice and thus the conclusions from the analyses presented in this study may not be extrapolated for weaker seasonal ice.

The raw IABP buoy positions are sampled irregularly in time with a mean time interval of 1 hour, and with errors ranging from 100 to 300 m depending on the positioning system they used (Thomas, 1999). Before being delivered to the scientific community, however, the buoy positions are interpolated in time (using a cubic function) to form an homogeneous trajectory dataset giving for each buoy its position every 12 hours. We manually checked each individual buoy track from the IABP dataset to clean them from unrealistic "jumps" or "spikes" in the trajectories and from obvious errors of the dating system. The unrealistic "jumps" present in buoy trajectories are either due to errors in the positioning system installed in the buoy or to wrong recordings during the deployment or recovery phase of the instruments. A polar stereographic projection is used to change the IABP and virtual buoy positions from geographic to Cartesian (x, y) coordinates.

2.2 Decomposition of the sea ice motion

The IABP buoy trajectories are geometrically complex, with abrupt changes in direction (Figure 1). Therefore, it is helpful to decompose the total sea ice motion into a mean part, that should be considered homogeneous and stationary, and a fluctuating part, that should contain the unpredictable, local or non-stationary motion. This is done here by following the classical approach used to study Lagrangian particle trajectories (see for example Zhang et al., 2001). This consists of splitting each trajectory into mean and fluctuating parts by using appropriate averaging scales L and T to compute the Lagrangian mean motion at any given location and time. An example for one particular IABP buoy trajectory is shown on Figure 2.

From the list of positions $\mathbf{x}_q^i$ of a buoy q, one can evaluate its position and velocity at time $\tilde{t}_q^i = \left(t_q^{i+1} + t_q^i\right)/2$ by computing:

$$\tilde{\mathbf{x}}_q^i = \left(\mathbf{x}_q^{i+1} + \mathbf{x}_q^i\right)/2, \tag{5}$$

$$\mathbf{u}_q^i = \left(\mathbf{x}_q^{i+1} - \mathbf{x}_q^i\right)/\Delta t. \tag{6}$$

By doing the same for all the available buoys, we build a dataset of 12-hourly velocities and positions, from which we compute the mean and fluctuating part of the motion.

The mean velocity field $\bar{\mathbf{u}}_{L,T}(\mathbf{x},t)$ is defined for any target position $\mathbf{x}$ and time t as

$$\bar{\mathbf{u}}_{L,T}(\mathbf{x},t) = \frac{1}{\sum_{q,i} w_q^i} \sum_{q,i} w_q^i \mathbf{u}_q^i, \tag{7}$$

where L and T are the spatial and temporal averaging scales and w_q^i are weight coefficients defined as in Rampal et al. (2009b), i.e. as a Gaussian function of the distance in space and time to the observations

$$w_q^i = \begin{cases} e^{-0.5\left(\frac{\|\tilde{\mathbf{x}}_q^i - \mathbf{x}\|^2}{L^2} + \frac{|\tilde{t}_q^i - t|^2}{T^2}\right)} & \text{if } \|\tilde{\mathbf{x}}_q^i - \mathbf{x}\| \leq L/2 \quad \text{and } |\tilde{t}_q^i - t| \leq T/2 \\ 0 & \text{else.} \end{cases} \tag{8}$$

In other words, the mean velocity is defined as a weighted average of all the 12-hourly velocities available in the dataset that are within a cercle of diameter L centred on the target position $\mathbf{x}$ and a time window of duration T centred on the target time t. The fluctuating velocities $\mathbf{u}'$ are then computed at each position $\tilde{\mathbf{x}}_q^i$ and time $\tilde{t}_q^i$ by subtracting the mean velocity $\bar{\mathbf{u}}_{L,T}(\tilde{\mathbf{x}}_q^i, \tilde{t}_q^i)$ from the total velocity $\mathbf{u}_q^i$. Both the mean and fluctuating velocities are then defined for a specific pair of averaging scales L and T.

To verify that the averaging scales, L and T, are well chosen, one can check that the ensemble average autocorrelation function of the fluctuating velocities rapidly decreases and remains close to 0 for long time interval τ, as shown in Figure 3 for $L = 400\,\text{km}$ and $T = 165$ days and the IABP dataset from 1979-2011. The ensemble average autocorrelation function χ is defined as

$$\chi(\tau) = \frac{1}{\sum_q T_{\max}^q} \sum_q T_{\max}^q C_q(\tau) \tag{9}$$

where $T^q_{\max}$ is the duration of each trajectory and C_q is the Lagrangian normalized autocorrelation function for each individual trajectory, which is defined as

$$C_q(\tau) = \frac{1}{\langle u'^2_q \rangle T^q_{\max}} \int_0^{T^q_{\max}} \mathbf{u}'_q(t)\mathbf{u}'_q(t+\tau)dt. \tag{10}$$

Here $\mathbf{u}'_q(t)$ is the fluctuating velocity of the buoys q at time t and $\langle u'^2 \rangle$ is the variance of the fluctuating velocities for the whole trajectory, which is defined as

$$\langle u'^2 \rangle = \langle u'^2_x(t) + u'^2_y(t) \rangle. \tag{11}$$

More generally, L and T are defined as the lowest scales for which the average integral time $\Gamma = \int \chi(\tau)d\tau$ remains quasi constant (i.e., less than 1% change). Since we cannot integrate this equation to infinity, the average integral time scale is computed as

$$\Gamma = \int_0^{t_0} \chi(\tau)d\tau \tag{12}$$

where t_0 is the first time $\chi(\tau)$ crosses zero (see for instance Poulain and Niiler, 1989; Rampal et al., 2009b). In the example of Figure 3, $t_0 = 6$ days, meaning that fluctuating velocities are uncorrelated for larger time scales, and the integral time scale Γ is equal to 1.5 days. Note that the diffusivity ($K = 1.0 \times 10^3\,\mathrm{m^2\,s^{-1}}$) for the example of Figure 3 is also given for information but will be discussed in Section 2.3. We checked by plotting Γ for different pairs of L and T (not shown) that a plateau is reached for averaging scales larger than $L = 400$ km and $T = 165$ days (as found in Rampal et al., 2009b, for the period 1979-2001), which are then the appropriate averaging scales for the data analysed here. These averaging scales are much smaller than the ones used by Colony and Thorndike (1984) to define a reference mean circulation, and this allows for a clear separation between the interannual variability and turbulent-like fluctuations due to synoptic scales activity of the atmosphere.

2.3 Application of Taylor's diffusion theory

Once the motion is decomposed into mean and fluctuating parts, it is possible to analyse the diffusion properties in the media by following the theory developed for turbulent fluids by Taylor (1921). Taylor's diffusion theory is valid for statistically steady and homogeneous turbulent flow without mean flow, and for which the fluctuating velocity follows a Gaussian distribution. When following a single particle in such conditions, the variance of its fluctuating displacement $\langle r'^2(t) \rangle$ should evolve as

$$\langle r'^2(t) \rangle = 2\langle u'^2 \rangle \int_0^t \int_0^{t_1} C(\tau)d\tau dt_1 \tag{13}$$

where $\langle u'^2 \rangle$, the variance of the fluctuating velocity, is constant in time.

For very long time intervals τ, the autocorrelation vanishes (as shown in Figure 3) and the integral of $C(\tau)$

$$\Gamma = \int_0^\infty C(\tau) d\tau. \tag{14}$$

is then a constant referred to as the Lagrangian integral time scale. Γ determines the transition between two diffusion regimes. For time much shorter than Γ, we are in the "ballistic" regime and Equation 13 becomes

$$\langle r'^2(t) \rangle = \langle u'^2 \rangle t^2, \qquad t \ll \Gamma \tag{15}$$

(this simply comes from the fact that $C(\tau)$ tends to the limiting value unity for small t). For time much longer than Γ, we are in the "Brownian" regime (also called "random walk" regime) and Equation 13 becomes

$$\langle r'^2(t) \rangle = 2\langle u'^2 \rangle \Gamma t + \alpha, \qquad t \gg \Gamma, \tag{16}$$

where α is a constant defined as $\alpha = -2\int_0^\infty \tau C(\tau) d\tau$ (LaCasce, 2008). This second regime is similar to the one driven by molecular diffusion (i.e., where fluctuating velocities are uncorrelated).

Following Lagrangian turbulent theory, diffusivity is defined as

$$K = \frac{1}{2} \frac{d\langle r'^2(t) \rangle}{dt}. \tag{17}$$

In the "ballistic" regime (with Equation 15), diffusivity increases with time and may be calculated as

$$K = \langle u'^2 \rangle t. \tag{18}$$

In the "Brownian" regime (with Equation 16), diffusivity (also called eddy diffusivity in that case) is constant and may be calculated as

$$K = \langle u'^2 \rangle \Gamma. \tag{19}$$

Note that the values of diffusivity for turbulent fluids are generally much larger than diffusion coefficients linked to molecular diffusion.

2.4 Results

One way to evaluate the results of the diffusion analysis is to look at the computed fluctuating displacement variance, $\langle r'^2(t) \rangle$, and to check if it fits with Taylor's theory. The fluctuating displacement is the integral in time of the fluctuating velocities and is here computed for segment periods of 35 days. As in Rampal et al. (2009b), we find a clear transition between the two diffusion regimes (indicated by the dashed lines in Figure 4). In the initial "ballistic" regime, the displacement variance grows with t^2, whereas in the "Brownian" regime, the displacement variance grows with t. The time

scale at which the regime transition occurs corresponds to the integral time scale, Γ, which value (1.4 days) is similar to the one found by Rampal et al. (2009b).

We continue the evaluation by comparing the magnitude of the fluctuating displacement variance to the asymptotic values predicted by the theory for $t \ll \Gamma$ (from Eq. 15) and for $t \gg \Gamma$ (from Eq. 16, neglecting the constant α) and we find a good match, whereas the magnitude presented in Rampal et al. (2009b) are underestimated by a factor 100. This mistake, which the authors of Rampal et al. (2009b) are aware of, simply comes from a wrong conversion factor and has no impact on the rest of their study, but is worth mentioning here, especially with regard to the coming discussion.

We also checked the stationarity of the variance of the fluctuating velocities and found that it was crucial for having a good match between the computed displacement variance and the asymptotic values predicted by the theory (not shown here). To increase the robustness and statistical significance of the diffusion analysis, we then artificially increase the number of buoy trajectories by splitting each trajectory into 35-day segments starting every 12 hours, i.e. every time a new buoy position along-track is available. By doing so, we make sure that the variance of the fluctuating velocities $\langle u'^2(t)\rangle$, where t here goes from 0 to 35 days, is almost constant. We checked that the relative deviation of $\langle u'^2(t)\rangle$ to the mean values $\langle u'^2\rangle$ is not larger than 10%.

This evaluation step ensures that the values given for $\langle u'^2\rangle$, Γ and K (see Table 2) are consistent with the theory and the analysed data, and can then been used with confidence. Note that the value of diffusivity given in Rampal et al. (2009b) is twice as low as the one found here and is not consistent with the other results presented in their study.

2.5 Discussion

The first outcome of the diffusion analysis is to provide a rigorous method to separate the mean circulation from the fluctuating motion, which can then be analysed separately. By using the right temporal averaging scales (about a season) on individual buoy trajectories, Thorndike and Colony (1982) were for example able to determine that the mean circulation is directly related to the mean geostrophic wind and the mean ocean circulation with equal contribution, whereas the fluctuating velocity variance is mainly explained (more than 70%) by the geostrophic wind.

The diffusion analysis also quantifies the diffusion properties of sea ice that can then be compared to the diffusion properties of passive tracers in the ocean. We note that the integral time scale Γ, as well as the diffusivity K are of the same order of magnitude as the ones found for ocean drifters (e.g., Poulain and Niiler, 1989; Zhang et al., 2001).

Another outcome of this analysis is to give a way to estimate the evolution of the fluctuating displacement, r'. The values of diffusivity and integral time scale can be used to evaluate the fluctuating displacement variance (and its standard deviation) for any time t with Equations 15 and 16. The standard deviation of the fluctuating displacement may be a crucial piece of information for the planning of a recovery operation in the case of drifting oil or some other pollutant that is trapped in

or attached to the ice, as it gives an estimate of how the size of the searching area around the predicted mean drift should increase through time, in a statistical sense. This is illustrated in Figure 5, which shows the evolution of the norm of the fluctuating displacement for every hundredth segment retrieved from the IABP trajectories for the winter periods from 1979 to 2011. This norm indicates the distance between a given buoy and the trajectory predicted by the mean drift. We checked that about 68.9%, 95.9% and 99.6% of the fluctuating displacements are smaller than 1, 2, and 3 standard deviations, which means that the fluctuating displacement distribution is in the Gaussian attraction basin.

If an operator can only trust the mean drift, which is the case for forecast longer than a few days, the information on the standard deviation could be used to define the size of the searching area around the position predicted by the mean drift. The searching area could be for example defined as a circular region with a radius equal to 3 standard deviations of the fluctuating displacement. The searching radius would then be about 90 km after 5 days (corresponding to a surface area of 23,600 km^2), and about 210 km after 30 days (corresponding to a surface area of 133,700 km^2). More examples are given in Table 1.

The diffusion analysis may also be used to predict long-term (typically seasonal) sea ice trajectories based on continuous or discrete tracer models. The average mean velocity needed by the tracer model may be defined from observations taken over the last few months, whereas the term reflecting the effects of the non-predictive fluctuations may be defined by the values of diffusivity and integral time scale derived from the diffusion analysis.

There are, however, some limitations when using the mean motion and mean diffusivity to force passive tracer models:

- the averaging smooths out local mean circulation features such as coastal currents,
- the method is not well suited for studying dispersion as it assumes no spatial correlation,
- the diffusivity could differ spatially and be not well represented by the basin-wide mean value,
- the diffusivity could be affected by the long term trend identified in Rampal et al. (2009a) and may therefore not be well represented by a value computed over the last four decades.

These issues do not occur if the tracer models are directly forced with sea ice velocity fields representing correctly both the mean and fluctuating parts of the motion field, as well as their gradient at all scales. The diffusion analysis presented here can also help to assess the representation of the mean and fluctuating parts. In the following section such an assessment is carried out on the results of two sea-ice(–ocean) modelling platforms, neXtSIM and TOPAZ.

3 Diffusion analysis on observed and simulated sea ice trajectories

Model output or reanalyses are often used to directly force passive tracer models (e.g. Nudds et al., 2013; Gearon et al., 2014). In that case, it is important to check if the simulated trajectories represent well the mean and fluctuating parts of the sea ice motion before pursuing an analysis of these trajectories. In some cases, a specific term is added to the tracer model (either via a diffusive term or a random perturbation) to represent the effect of the unresolved physics on the tracer evolution. When applied in the ocean, the stochastic part represents molecular and turbulent diffusive processes that are not included in the velocity fields simulated by the ocean model. However, as sea ice in the ice pack does not behave as a turbulent fluid, the stochastic term to be used for sea ice should not be taken to represent the same underlying physical processes as in the ocean, and therefore may have a different form and/or be scaled with a different coefficient. In this section, we follow an approach that is frequently used for the oceanic drifters (e.g., Dominicis et al., 2012) and which consists of applying the diffusion analysis to observed and simulated trajectories to determine how the mean and fluctuating motion are represented and how unresolved physics could be taken into account.

3.1 Observed and simulated trajectories datasets

In this section we compare observed trajectories from the IABP dataset to trajectories of virtual buoys (here called "floats") whose motion is forced by sea ice fields coming from two different model setups. Due to limited available computational time, this analysis is restricted to three consecutive winters. The period 2007-2010 has been selected for its relatively good data coverage, with more than 40 IABP buoys recording their positions simultaneously every day.

The float simulations are initialised at the same time and position as the IABP buoys (280 individual floats). The positions of each float are sampled every 12 hours, and stop when the IABP buoy track stops or when the float enters into an area of simulated open water (sea ice concentrations less than 15%). By doing so, three comparable datasets are obtained: i) the observed sea ice trajectories, already discussed in section 2.1, ii) the trajectories of virtual sea ice floats forced by a free run of the TOPAZ sea-ice–ocean data assimilation system, and iii) the trajectories of virtual sea ice floats simulated by the neXtSIM sea ice model.

3.1.1 TOPAZ trajectories dataset

TOPAZ is a coupled sea-ice–ocean data assimilation system (Sakov et al., 2012) used in the operational Arctic Ocean forecast platform of the European Copernicus Marine Environment Monitoring service (http://marine.copernicus.eu). It has also been used to build a 23-years reanalysis (1991-2013), also distributed by the Copernicus marine service. The ocean part of TOPAZ uses the HYCOM model version 2.2, with 28 vertical layers, whereas the sea ice part uses a one thickness category sea ice model whose thermodynamics are described in Drange and Simonsen (1996) and

dynamics are built around a standard EVP rheology (Hunke and Dukowicz, 1997) as it was implemented in the CICE sea ice model (the Los Alamos Sea Ice Model) version 4 (Hunke and Lipscomb, 2010).

The sea-ice–ocean model of TOPAZ (hereafter called the TOPAZ model) is run here in free-run mode (i.e., no data assimilation is applied) in the same configuration as in Sakov et al. (2012). The model grid covers the Arctic and North-Atlantic Oceans with a mean resolution of approximately 12 km over the Arctic. The three TOPAZ simulations used here start on September 15^{th} and finish on May 15^{th} for three consecutive winters from 2007 to 2010 with initial conditions coming from the free-run simulation described in Sakov et al. (2012). The applied atmospheric forcing fields are the 6-hourly 10-meter wind velocities from the ERA interim reanalysis (ERAi) distributed at 80 km spatial resolution (http://www.ecmwf.int/en/research/climate-reanalysis/era-interim, ECMWF (2011)).

The TOPAZ model in free run has been evaluated in Sakov et al. (2012) and was found to overestimate sea ice drift by about 3 km day^{-1} compared to buoy data. To try to solve this issue, the frictional drag parameters for the atmosphere-ice stress has been reduced to $c_a = 0.0016$ in the TOPAZ operational platform (not yet documented) and we then use this value here. The mean sea ice thickness in the free run is underestimated and typically shows too thin ice in areas of thick ice and inversely, too thin ice in areas of thick ice. The sea ice thickness is slightly better in the TOPAZ reanalysis but the total volume is still too low (Sakov et al., 2015, http://marine.copernicus.eu/documents/QUID/CMEMS-ARC-QUID-002-003.pdf). The TOPAZ model has been found “sufficiently eddy permitting" in the North Atlantic but this does not apply to the Arctic where the Rossby radius is about 5–15km in the Nansen and Canadian basins and can be as small as 1–7 km in the shelf seas where density stratification is weak or in shallow waters (Nurser and Bacon, 2014).

The float tracking with the TOPAZ model is here performed off-line by using the hourly sea ice velocity fields simulated by the model. The float-tracking system moves the floats with a simple Eulerian method. The virtual floats move in the quasi-homogeneous TOPAZ Arctic grid in order to avoid singularity errors at and around the Pole that would arise with a regular longitude/latitude grid. The sea ice velocities given by the TOPAZ model are interpolated with a bilinear method to the position of the virtual Lagrangian floats every hour. We checked that for the time scale and spatial resolution considered here, this tracking method gives similar results to using an online tracking system, with the advantage of remaining computationally efficient.

3.1.2 neXtSIM trajectories dataset

neXtSIM is a fully-Lagrangian thermodynamic-dynamic sea ice model, using an adaptive finite element mesh and a mechanical framework based on the elasto-brittle rheology (Rampal et al., 2015). Thermodynamic growth and melt of the ice are based on the zero-layer model of Semtner (1976) and the ice model is coupled to a slab ocean model, whose variables are the slab ocean temperature and

salinity. The model is still under development but is already used in an experimental sea ice forecast platform covering the Kara Sea (https://www.nersc.no/data/nextsim-f).

The configuration used here is the same as the one presented and evaluated in Rampal et al. (2015). The model domain shares the exact same coastlines and open boundaries as the TOPAZ model described above, i.e. it covers the Arctic and North-Atlantic Oceans extending from an open boundary at 43°N in the North-Atlantic to an open boundary in the Bering Strait. The mean resolution of the finite element mesh used by neXtSIM is about 10 km. The three neXtSIM simulations used here start on September 15$^{\mathrm{th}}$ and finish on May 15$^{\mathrm{th}}$, for three consecutive winters from 2007 to 2010. The model is initialised with the ice concentration derived from the AMSR-E passive microwave sensor (Kaleschke et al., 2001; Spreen et al., 2008, data obtained from the Integrated Climate Date Center, University of Hamburg, Germany, http://icdc.zmaw.de) and the TOPAZ ice thickness, within the area reported by AMSR-E as being covered with ice. The modelled ice volume in the TOPAZ reanalysis being known too low (Sakov et al., 2015) we increased the initial thickness uniformly so that the total volume is the same as that given by the PIOMAS model on September 15$^{\mathrm{th}}$ 2007, 2008 and 2009, respectively (Zhang and Rothrock, 2003). The good performance of PIOMAS in simulating Arctic sea ice volume as compared to available observations is reported in Schweiger et al. (2011). The temperature and salinity of the slab ocean model are initialised with temperature and salinity from TOPAZ. The model is forced with the ocean state (i.e., sea surface height, velocity at 30 m depth, and sea surface temperature and salinity) of the TOPAZ reanalysis. The atmospheric state comes from the Arctic System Reanalysis, Interim version (ASR-Interim hereafter) (http://rda.ucar.edu/datasets/ds631.4/, Byrd Polar Research Centre/The Ohio State University (2012). Accessed 01 Jan 2014). The ASR-Interim is a high resolution atmospheric reanalysis (30 km) known to reproduce particularly well the near-surface wind fields in the Arctic region (Bromwich et al., 2016).

The neXtSIM model is able to simulate correctly the observed evolution of the sea ice volume, extent and area for the freezing season (from September to May) but simulates a too rapid melt from May (Rampal et al., 2015). This limitation does not impact the results of this analysis as we only look at simulated drift in winter with simulations restarted every September. For the winter season 2007-2008, the simulated drift fields have been extensively evaluated in Rampal et al. (2015) against satellite derived products, showing no bias in the 3-days drift and a good representation of the mean circulation.

The float tracking with neXtSIM is performed at run time. The main reason for doing this is that the Lagrangian advection used in the neXtSIM model offers some additional challenges to a post-processing approach using Eulerian fields. The floats positions then change as the underlying mesh moves and are interpolated onto the new mesh after each remeshing step (see Rampal et al. (2015) for more details on the remeshing procedure).

3.2 Results

Figure 6 shows the maps with all the buoy trajectories for each winter season from the IABP, TOPAZ and neXtSIM ice trajectories datasets. The different datasets for the period 2007 to 2010 are much sparser and cover a smaller portion of the Arctic Ocean than the reference dataset analysed in Section 2.1. As it is not practical to directly compare the simulated and observed trajectories, we analyse separately the mean drift and the fluctuating part of the motion by applying the same decomposition of the sea ice motion as the one presented in Section 2.1.

The mean velocity fields for each winter season and for the three datasets are shown in Figure 7. The two main features of the Arctic-wide mean circulation are the Beaufort Gyre and the Transpolar Drift. However, we note that the strength and the extent of the Beaufort Gyre, as well as the strength of the Transpolar drift, vary from one year to the other. This inter-annual variability is well represented by both TOPAZ and neXtSIM. The two models, however, perform differently in terms of the magnitude and the spatial distribution of the mean sea ice drift. The TOPAZ model generally overestimates the mean drift field and does not correctly reproduce the spatial patterns. In particular the size of the Beaufort Gyre is often overestimated and the model does not reproduce the low drift speed along the Canadian Arctic Archipelago, which are due to significantly thicker and more ridged ice. The mean ice drift simulated by the neXtSIM model reproduces well the mean circulation patterns, slightly underestimates the magnitude of the Beaufort Gyre but reproduces well the almost immobile pack ice north of the Canadian Arctic Archipelago.

The statistical distribution of the mean velocity also gives valuable information and can be used to evaluate the simulated mean drift. Figure 8 shows the probability density function of the mean speed, $\bar{U} = \sqrt{\bar{u}^2 + \bar{v}^2}$, as computed from the IABP buoy data and from the TOPAZ and neXtSIM virtual buoy data for the period 2007-2010. The mean speed distribution from the observations fits well with an exponential function and has a mean value equal to $2.45\,\mathrm{cm\,s^{-1}}$. The mean speed distribution obtained with the TOPAZ dataset does not follow an exponential distribution and has a mean value equal to $3.38\,\mathrm{cm\,s^{-1}}$, which is about 38% larger than the one of the IABP buoys. The mean velocities obtained from the neXtSIM dataset follow an exponential distribution with a mean equal to $2.00\,\mathrm{cm\,s^{-1}}$, which is about 18% lower than the observations.

When removing the mean part of the velocity field we are left with the fluctuating velocity field $u'(x)$. If the mean part is removed correctly (according to the Taylor's theory), the fluctuating velocities should be symmetrically distributed around zero. This is the case in our results (not shown), meaning that one can directly look at the speed without losing information. The PDFs of the fluctuating speeds are plotted in Figure 9 with the Gaussian and exponential fits indicated for reference.

The fluctuating speeds of the IABP buoys follow an exponential distribution with a mean equal to $6.9\,\mathrm{cm\,s^{-1}}$. It is important to note here that the data follow an exponential distribution instead of a Gaussian distribution, this means that the sea ice fluctuating speed can be much larger than a standard deviation away from the (zero) mean. Such non-Gaussian distributions for fluctuating speeds are not

expected for fully developed turbulence (Batchelor, 1960; Frisch, 1995) but have been observed for oceanic surface currents during energetic events associated with large organised structures such as jets and vortices. Such a signature for multi-year sea ice may indicate that sea ice dynamics are dominated by the passage of large perturbations over the Arctic, whereas less energetic features have less impact on sea ice motion. This selective sensitivity to energetic events may be related to the intrinsic properties of solids associated with threshold mechanics (Rampal et al., 2009b). This seems to be supported by the fact that for weaker seasonal sea ice, the observed fluctuating velocities rather follow Gaussian statistics (Lukovich et al., 2011).

The fluctuating speeds from the TOPAZ setup are too high on average (by about 30%) with a mean value close to 9 cm s^{-1}, and their statistics do not follow an exponential distribution. The fluctuating speeds from neXtSIM are slightly too low (by about 10%) with a mean value equal to 6.1 cm s^{-1} and follow an exponential distribution within the range 0 to 30 cm s^{-1}.

Figure 10 shows the evolution of the fluctuating displacement variance for the observed and simulated trajectories. The fluctuating displacement are here computed for segments of 35 days, the same as in the analysis of the reference dataset. The magnitude of the fluctuating displacement variance is constantly overestimated in TOPAZ, by about 40% in the ballistic regime and almost 100% in the Brownian regime. This is consistant with the fact that both the integral time scale and fluctuating velocity variance are overestimated by about 40% (see Table 2). In the Brownian regime, these overestimation are combined resulting in the overestimation of the diffusivity by about 100%. In neXtSIM the fluctuating displacements are underestimated in the ballistic regime but correctly reproduced for the Brownian regime. This is consistent with the underestimation of the fluctuating velocities variance by about 20%, which is balanced in the Brownian regime by the overestimation of the integral time scale by about 20%, leading to a diffusivity almost equal to the one coming from the observations for the same period.

Figure 11 shows the regional distribution of the diffusivity fields. The diffusivity computed from the IABP buoys is not uniform and seems to be related to the spatial distribution of the multi-year ice concentration and ice thickness (as shown in Kwok et al., 2009), with rather low diffusivity values along the Canadian Arctic Archipelago (i.e. down to about $0.5 \times 10^3\,\mathrm{m^2 s^{-2}}$) and larger values in the East Siberian Sea and in Beaufort Sea. The presence of thick multi-year ice (more than 3 meters) north of the CAA may then explain the low diffusivity values (lower than $1 \times 10^3\,\mathrm{m^2 s^{-2}}$).

The results obtained with the TOPAZ setup analysed here also show a non-uniform distribution that may be related to the simulated sea ice thickness pattern (not shown). The magnitude of the diffusivity for TOPAZ is overestimated almost everywhere except for a few cells located at the boundaries of the analysed domain. The results obtained with the neXtSIM setup represent well the magnitude and spatial variability of the diffusivity. The correlation coefficient between the diffusivity map obtained from observations and those obtained from TOPAZ and neXtSIM are equal to 0.7 and 0.85, respectively.

3.3 Discussion

The TOPAZ model reproduces the very basic characteristics of the Arctic sea ice mean circulation, with interannually varying Beaufort Gyre and Transpolar drift. The largest differences in the mean circulation simulated by TOPAZ and the observations are localised north of the CAA in a region covered by thick multi-year ice. These differences appear to be related to the local underestimation of sea ice thickness by the TOPAZ model. This localised underestimation of the mean drift greatly affects the lower part of the distribution (mean drift lower than $5\,\mathrm{cm\,s^{-1}}$). The misrepresentation of the sea ice thickness distribution in the Arctic by TOPAZ is likely not a problem related to the sea ice thermodynamics model but rather to the sea ice dynamics model and more specifically to its rheological component which controls the formation of leads and ridges by determining the mechanical response of the ice pack to external mechanical forcings.

The largest values of the mean circulation (mean drift larger than $15\,\mathrm{cm\,s^{-1}}$) are underestimated in TOPAZ. Those values are localised in regions of thinner ice, where the TOPAZ system is known to overestimate sea ice thickness. This underestimation could also be due to the ocean model, especially in the Beaufort Gyre, which is reported as being too large and misplaced in TOPAZ compared to observations (Sakov et al., 2012).

Contrary to the mean drift, the long term fluctuating displacement (and equivalently the diffusivity) is homogeneously overestimated in TOPAZ. The large overestimation (by about 100%) of the long term fluctuating displacement comes from the combined effect of an excessively long integral time scale and overestimated fluctuating velocities variance. The overestimation of the integral time scale is likely due to the atmospheric forcing (ERA-interim), which has a limited representation of the local and rapidly varying surface wind.

The simulations with the neXtSIM model represent well the spatial and statistical distribution of the mean circulation. The nearly immobile ice north of the CAA is well represented. The largest values of the mean circulation (mean drift larger than $15\,\mathrm{cm\,s^{-1}}$) are underestimated, just as in TOPAZ, and this may explain the slight underestimation of the averaged mean drift. This misrepresentation may thus come from the oceanic forcing which comes from the TOPAZ reanalysis.

The spatial and statistical distributions of the fluctuating motion are also well reproduced in the neXtSIM simulations. The slight underestimation of the averaged fluctuating speed likely comes from the missing largest values of fluctuating velocities. This, as well as the overestimation of the integral time scale, is likely to come from missing local and rapidly varying high winds in the atmospheric reanalysis ASR-interim, used here to force neXtSIM. It may also come from missing physics related to the absence of mechanical coupling between neXtSIM and the slab ocean underneath in our configuration. Therefore, sea ice motion features like inertial oscillations that impact 12-hourly drift statistics are not reproduced in the simulations analysed for this study.

It is common practice to add an extra diffusive term to the tracer evolution equation, as discussed earlier. In the case of the TOPAZ setup, adding such an extra term to the tracer evolution equation

would not help, as the model already overestimates the fluctuation both in the ballistic and Brownian regimes. Adding such a term when using the neXtSIM setup presented here may improve the evolution of the fluctuating displacement in the ballistic regime. Adding a random term would increase the fluctuating velocity variance but decrease the integral time scale. Doing this may then keep the good performance in reproducing the long term displacements and diffusivity fields, without impacting the long term mean drift.

4 Summary and conclusions

In the first part of the paper (Section 2), we analyse IABP buoys trajectories for the winter periods between 1979 and 2011 and we confirm that the appropriate averaging scales to define the mean circulation in winter are about 400 km and 165 days. This agrees with the results of Rampal et al. (2009b), but we additionally verify that the computed displacement variance is consistent with the theory and with the estimated values of the integral time scale (about 1.5 days), the 12-hourly fluctuating velocities variance (73 $\mathrm{km^2\,day^{-2}}$) and the diffusivity ($1.2\times10^3\,\mathrm{m^2 s^{-2}}$).

These information can be used in the context of pollutant tracking to evaluate the proper size for the searching area around the long-term trajectory predicted by the mean drift. If one defines the searching area as a circular region with a radius equal to 3 standard deviations of the fluctuating displacement, we find that on average the searching radius should be about 90 km after 5 days (corresponding to a surface area of 24000 $\mathrm{km^2}$), and about 210 km after 30 days (corresponding to a surface area of 134000 $\mathrm{km^2}$).

The estimates of the mean drift field, diffusivity and integral time scale computed here could also be used within a passive tracer model (either with an advection-diffusion equation or a Lagrangian stochastic approach) to estimate the probability for a particle to be in a given position after a given time. The limitations of that approach would be the excessive smoothing of local mean circulation patterns (e.g., coastal currents), the inability to represent dispersion and the potential misrepresentation of the spatial and temporal distribution of the diffusivity values.

In the second part of the paper (Section 3), we analyse trajectories of virtual buoys whose motion is forced by simulated sea ice velocity fields. This approach eliminates the limitations of using tracer models forced by mean fields but relies on the good representation of the sea ice drift by the models. To illustrate how one could evaluate sea ice model outputs before using them for trajectory modelling, we applied the diffusion analysis to three similar datasets, one from the IABP data, one from the TOPAZ model and one from the neXtSIM model, and we compared the numbers obtained from simulated and observed trajectories.

The mean velocities in the simulations using TOPAZ are on average 40% too high, follow a Gaussian instead of an exponential distribution and do not represent correctly the circulation near the Canadian Arctic Archipelago. This limitation may be largely linked to the misrepresentation of the

sea ice thickness spatial distribution, with too thin ice along the CAA and too thick ice elsewhere. The fluctuating velocities mean and variance are also overestimated, even if the simulated fields do not reproduce the observed high values of fluctuating speed (larger than $40\,\mathrm{cm\,s^{-1}}$). The overestimation of the fluctuating velocities combined to the overestimation of the integral time scale leads to an overestimation of the long-term displacement variance by about 100%. The validity of tracer studies based on similar setups could be substantially affected by those differences compared to observations.

The mean velocities in the simulations using neXtSIM are on average 20% too low, follow an exponential distribution and reproduce well the spatial distribution of the mean motion. The fluctuating velocity's mean and variance are also slightly underestimated, which may come from the missing high values of fluctuating speed (larger than $40\,\mathrm{cm\,s^{-1}}$). The underestimation of the fluctuating variance is compensated by the overestimation of the integral time scale, leading to long-term displacement variance fitting very well the observations. Tracer studies based on similar results could be trusted except for the ballistic regime (first few days), where the simulated displacement variance is too weak.

As a follow up of this study, it would be interesting to investigate the causes of the missing high velocities and the overestimation of the integral time scale, first by looking at the impact of the atmospheric forcing resolution and second by looking at the representation of the inertial/tidal oscillations by the two modelling platforms used here. To better asses the quality of the simulated sea ice dynamics, it would be interesting to also perform a dispersion analysis as in Rampal et al. (2008) or to specifically study sea ice deformation as in Bouillon and Rampal (2015) with data from models and observations. Finally, it is worth noting that the representation of the mean sea ice circulation depends on many processes (mean circulation of the ocean, spatial and temporal variation of the ocean–ice and air–ice drag coefficients as a function of the ice age/type, representation of the ocean–ice and atmosphere–ice boundary layers (McPhee, 2012), etc.), whose the respective roles would also need to be further explored.

Acknowledgements. We would like to acknowledge L. Bertino, J. Xie and P. Griewank for interesting discussions and their contribution to the development of TOPAZ and neXtSIM. We also thank T. Williams for his help improving the manuscript. This work was supported by fundings from the Oil and Gas Producers (OGP), TOTAL E&P and the Research Council of Norway via the SIMech project (No. 231179/F20, 2014-2016).

References

Batchelor, G. K.: The theory of homogeneous turbulence, Students' edition. By G. K. Batchelor. Cambridge Monographs on Mechanics and Applied Mathematics. Cambridge (University Press), 1959. Pp. xi, 197; 28 Figures; 18s. 6d, Quarterly Journal of the Royal Meteorological Society, 86, 291–291, 1960.

Borgå, K., Poltermann, M., Polder, A., and Pavlova, O.: Influence of diet and sea ice drift on organochlorine bioaccumulation in Arctic ice-associated amphipods, Environmental Pollution, 117, 47–60, doi:10.1016/s0269-7491(01)00160-9, 2002.

Bouillon, S. and Rampal, P.: Presentation of the dynamical core of neXtSIM, a new sea ice model, Ocean Modelling, 91, 23–37, 2015.

Bromwich, D. H., Wilson, A. B., Bai, L.-S., Moore, G. W. K., and Bauer, P.: A comparison of the regional Arctic System Reanalysis and the global ERA-Interim Reanalysis for the Arctic, Quarterly Journal of the Royal Meteorological Society, 142, 644–658, doi:10.1002/qj.2527, http://dx.doi.org/10.1002/qj.2527, 2016.

Colony, R. and Thorndike, A. S.: An estimate of the mean field of Arctic sea ice motion, J. Geophys. Res., 89, 10 623—10 629, doi:10.1029/JC089iC06p10623, 1984.

Colony, R. and Thorndike, A. S.: Sea ice motion as a drunkard's walk, J. Geophys. Res., 90, 965–974, 1985.

Dominicis, M., Leuzzi, G., Monti, P., Pinardi, N., and Poulain, P.-M.: Eddy diffusivity derived from drifter data for dispersion model applications, Ocean Dynamics, 62, 1381–1398, doi:10.1007/s10236-012-0564-2, http://dx.doi.org/10.1007/s10236-012-0564-2, 2012.

Drange, H. and Simonsen, K.: Formulation of air-sea fluxes in the ESOP2 version of MICOM, Tech Rep. 125, Tech. rep., NERSC, Bergen, Norway, www.nersc.no, 1996.

Drozdowski, A., Nudds, S., Hannah, C. G., Niu, H., Peterson, I., and Perrie, W.: Review of Oil Spill Trajectory Modelling in the Presence of Ice, Tech. rep., Canadian Tech. Rep. Hydrogr. Ocean Sci. 274, 2011.

Fowler, C. W., Maslanik, J. A., and Emery, W. J.: Satellite-Derived Evolution of Arctic Sea Ice Age: October 1978 to March 2003, IEEE Geosci. Remote Sensing Lett., 1, 71–74, 2004.

Frisch, U.: Turbulence: The Legacy of A. N. Kolmogorov, Cambridge University Press, U.K., 1995.

Gearon, M., French McCay, D., Chaite, E., Zamorski, S., Reich, D., Rowe, J., and Schmidt-Etkin, D.: SIMAP Modelling of Hypothetical Oil Spills in The Beaufort Sea for World Wildlife Fund (WWF), Tech. rep., Applied Science Associates and Environmental Research Consulting (ERC), South Kingstown, RI and Cortlandt Manor, NY P13-235, http://awsassets.wwf.ca/downloads/wwf_beaufort_sea_oil_spill_modelling_full_report_rps_asa.pdf, final Report, 2014.

Hunke, E. C.: Sea ice volume and age: Sensitivity to physical parameterizations and thickness resolution in the CICE sea ice model, Ocean Modelling, 82, 45–59, 2014.

Hunke, E. C. and Dukowicz, J. K.: An elastic-viscous-plastic model for sea ice dynamics, J. Phys. Ocean., 27, 1849–1867, 1997.

Hunke, E. C. and Lipscomb, W. H.: CICE model Ver. 4.1 Documentation, Tech. rep., T-3 Fluid Dynamics Group, Los Alamos National Laboratory, 2010.

Kaleschke, L., Lüpkes, C., Vihma, T., Haarpaintner, J., Bochert, A., Hartmann, J., and Heygster, G.: SSM/I Sea Ice Remote Sensing for Mesoscale Ocean-Atmosphere Interaction Analysis, Canadian Journal of Remote Sensing, 27, 526–537, 2001.

Kwok, R., Cunningham, G. F., Wensnahan, M., Rigor, I., Zwally, H. J., and Yi, D.: Thinning and volume loss of the Arctic Ocean sea ice cover: 2003–2008, Journal of Geophysical Research: Oceans, 114, doi:10.1029/2009JC005312, c07005, 2009.

LaCasce, J. H.: Statistics from Lagrangian observations, Prog. Oceanogr., 77, 1–29, 2008.

Lukovich, J. V., Babb, D. G., and Barber, D. G.: On the scaling laws derived from ice beacon trajectories in the southern Beaufort Sea during the International Polar Year - Circumpolar Flaw Lead study, 2007–2008, Journal of Geophysical Research: Oceans, 116, doi:10.1029/2011JC007049, c00G07, 2011.

Lukovich, J. V., Hutchings, J. K., and Barber, D. G.: On sea-ice dynamical regimes in the Arctic Ocean, Annals of Glaciology, 56, 323–331, 2015.

McPhee, M. G.: Advances in understanding ice-ocean stress during and since AIDJEX, Cold Regions Science and Technology, 76-77, 24–36, 2012.

Nudds, S. H., Drozdowski, A., Lu, Y., and Prinsenberg, S.: Simulating Oil Spill Evolution in Water and Sea Ice in the Beaufort Sea, in: Proceedings of the twenty-third International Offshore and Polar Engineering, pp. 1066–1071, International Society of Offshore and Polar Engineers, 2013.

Nurser, A. J. G. and Bacon, S.: The Rossby radius in the Arctic Ocean, Ocean Science, 10, 967–975, 2014.

Pfirman, S., Eicken, H., Bauch, D., and Weeks, W.: The potential transport of pollutants by Arctic sea ice, Science of The Total Environment, 159, 129–146, doi:http://dx.doi.org/10.1016/0048-9697(95)04174-Y, 1995.

Poulain, P.-M. and Niiler, P. P.: Statistical analysis of the surface circulation in the California Current System using satellite-tracked drifters, J. Phys. Ocean., 19, 1588–1603, 1989.

Rampal, P., Weiss, J., Marsan, D., Lindsay, R., and Stern, H.: Scaling properties of sea ice deformation from buoy dispersion analysis, Journal of Geophysical Research: Oceans, 113, n/a–n/a, doi:10.1029/2007JC004143, http://dx.doi.org/10.1029/2007JC004143, c03002, 2008.

Rampal, P., Weiss, J., and Marsan, D.: Positive trend in the mean speed and deformation rate of Arctic sea ice, 1979-2007, Journal of Geophysical Research: Oceans, 114, n/a–n/a, doi:10.1029/2008JC005066, http://dx.doi.org/10.1029/2008JC005066, c05013, 2009a.

Rampal, P., Weiss, J., Marsan, D., and Bourgoin, M.: Arctic sea ice velocity field: General circulation and turbulent-like fluctuations, Journal of Geophysical Research: Oceans, 114, C10 014, 2009b.

Rampal, P., Bouillon, S., Ólason, E., and Morlighem, M.: neXtSIM: a new Lagrangian sea ice model, The Cryosphere Discussions, 9, 5885–5941, doi:10.5194/tcd-9-5885-2015, http://www.the-cryosphere-discuss.net/9/5885/2015/, 2015.

Rigor, I. and Colony, R.: Sea-ice production and transport of pollutants in the Laptev Sea, 1979–1993, Science of The Total Environment, 202, 89–110, doi:http://dx.doi.org/10.1016/S0048-9697(97)00107-1, environmental Radioactivity in the Arctic, 1997.

Sakov, P., Counillon, F., Bertino, L., Lisæter, K. A., Oke, P., and Korablev, A.: TOPAZ4: An ocean sea ice data assimilation system for the North Atlantic and Arctic, Ocean Sci., 8, 633–662, doi:10.5194/osd-9-1519-2012, 2012.

Sakov, P., Counillon, F., Bertino, L., Finck, N., and Renkl, C.: Quality Information Document For Arctic Physical Reanalysis Product, Tech. rep., EU Copernicus Marine Service, Bergen, 2015.

Schweiger, A., Lindsay, R., Zhang, J., Steele, M., Stern, H., and Kwok, R.: Uncertainty in modeled Arctic sea ice volume, Journal of Geophysical Research: Oceans, 116, doi:10.1029/2011JC007084, c00D06, 2011.

Semtner, A. J.: A model for the thermodynamic growth of sea ice in numerical investigations of climate, J. Phys. Ocean., 6, 379–389, 1976.

Spreen, G., Kaleschke, L., and Heygster, G.: Sea ice remote sensing using AMSR-E 89-GHz channels, Journal of Geophysical Research: Oceans, 113, doi:10.1029/2005JC003384, c02S03, 2008.

Taylor, G. I.: Diffusion by Continuous Movements, Proceedings of The London Mathematical Society, s2-20, 196–212, doi:10.1112/plms/s2-20.1.196, 1921.

Thomas, D.: The quality of sea ice velocity estimates, Journal of Geophysical Research: Oceans, 104, 13 627–13 652, 1999.

Thorndike, A. S. and Colony, R.: Sea ice motion in response to geostrophic winds, J. Geophys. Res., 87, 5845–5852, 1982.

Zhang, H., Prater, M. D., and Rossby, T.: Isopycnal Lagrangian statistics from the North Atlantic Current RAFOS float observations, J. Geophys. Res., 106, 13 817, 2001.

Zhang, J. and Rothrock, D.: Modeling global sea ice with a thickness and enthalpy distribution model in generalized curvilinear coordinates, Monthly Weather Review, 131, 845–861, 2003.

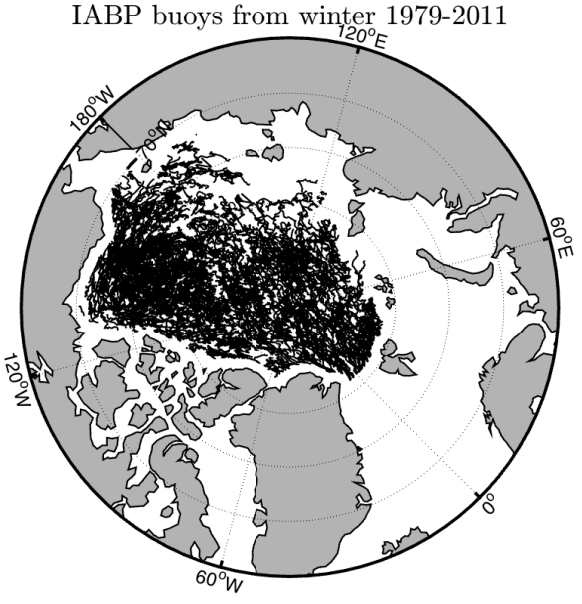

Figure 1. Buoy tracks from the IABP dataset for the period 1979–2011.

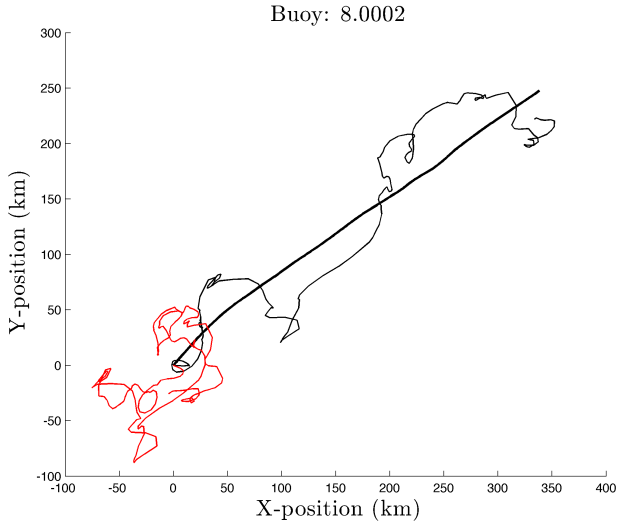

Figure 2. Example of a 35-days long trajectory from a buoy of the IABP dataset (thin black line) partitioned into a mean (thick black line) and fluctuating (red line) parts using the method described in subsection 2.2. The starting point of the three trajectories is the same and arbitrarily set to be the origin of the axes.

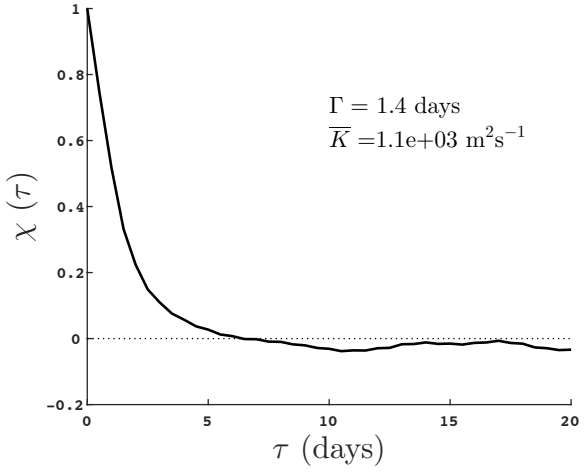

Figure 3. Ensemble averaged fluctuating velocity autocorrelation function for the IABP dataset for winter seasons 1979 to 2011. The values of the integral time scale Γ and mean horizontal diffusivity $\bar{K}$ for this particular period are indicated.

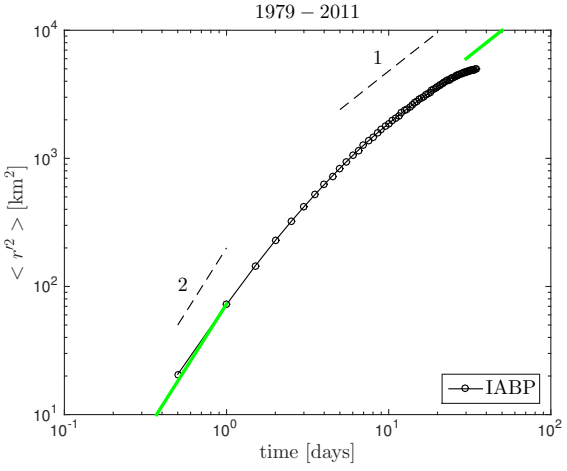

Figure 4. Ensemble mean of the variance of the fluctuating displacement $< r'^2 >$ for the winter seasons 1979-2011 for IABP. The dashed lines indicate the theoretical slopes for the two diffusion regimes: the "ballistic" regime ($\langle r'^2(t)\rangle \sim t^2$) which has a slope equal to 2, and the "Brownian" regime ($\langle r'^2(t)\rangle \sim t$) which has a slope equal to 1. The green lines correspond to the equations 15 and 16 and are shown for reference.

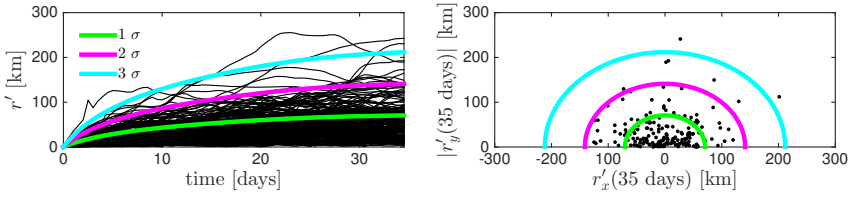

Figure 5. Time evolution of the norm of the fluctuating displacement r' for every hundredth 35-days segments extracted from the IABP buoys tracks for the winters 1979-2011 (left). The solid lines in color indicate 1, 2 and 3 standard deviations of the fluctuating displacement, respectively. Illustration of searching area after 35 days (right) estimated statistically from the IABP buoys dataset for the period 1979-2011.

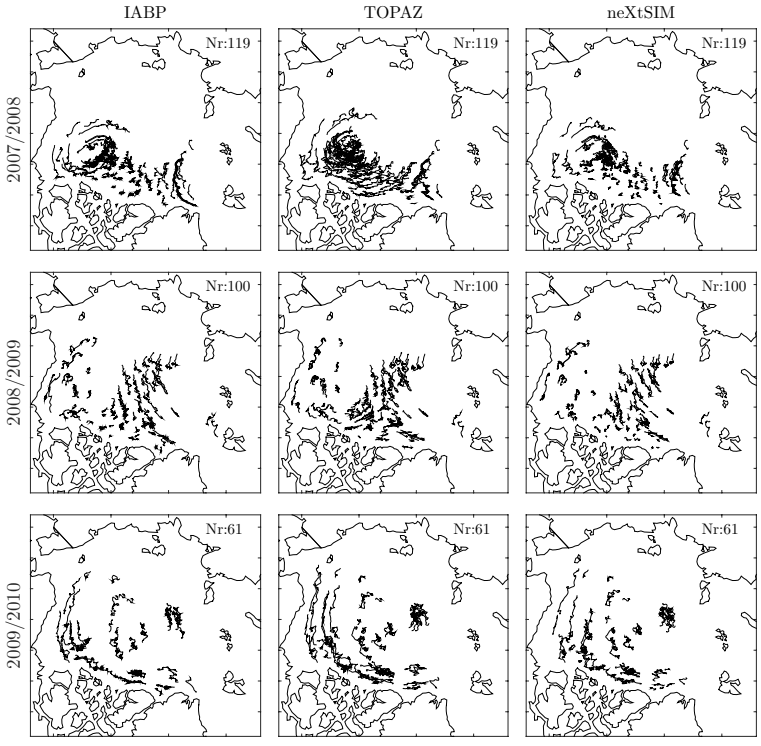

Figure 6. IABP buoys tracks (left) and their corresponding virtual tracks simulated by TOPAZ (centre) and neXtSIM (right) for the winters 2007/2008 (top), 2008/2009 (middle), and 2009/2010 (bottom).

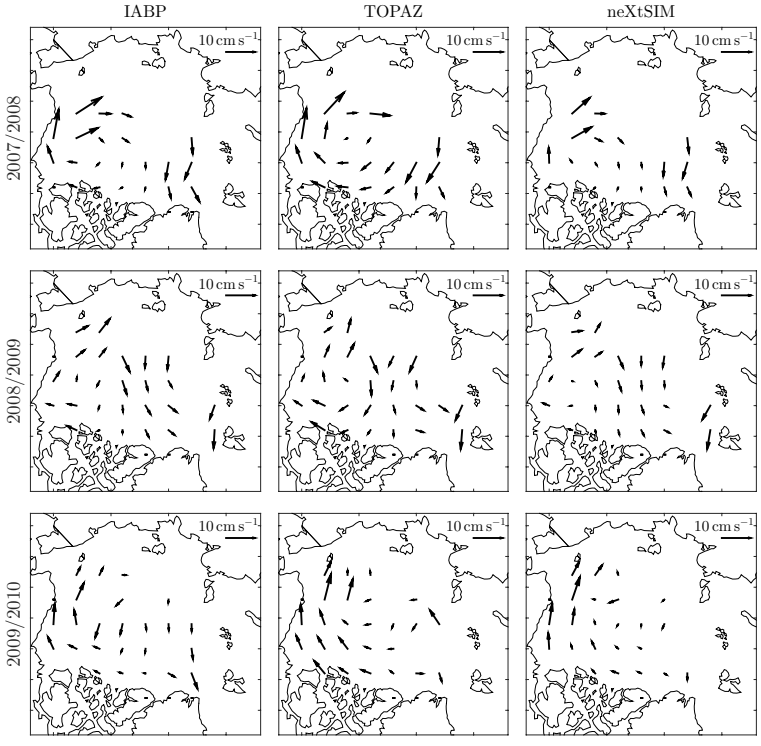

Figure 7. Mean sea ice velocity field computed from the IABP buoys dataset (left) and the corresponding floats dataset generated with TOPAZ (centre), and neXtSIM (right) for the winters 2007/2008 (top), 2008/2009 (middle), and 2009/2010 (bottom). The mean velocity vectors are shown on a 400×400 km regular grid.

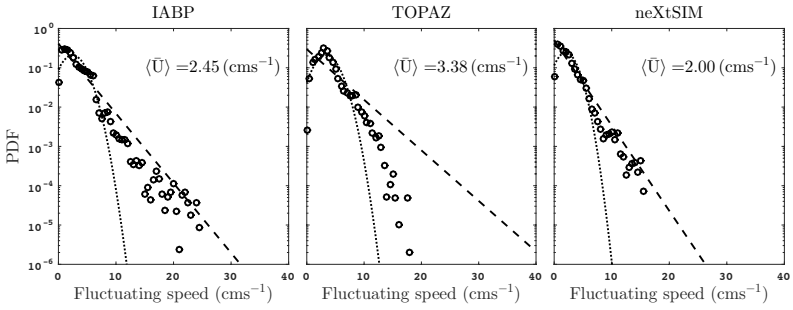

Figure 8. Probability density function of the mean speed of the IABP buoys (left), and of the corresponding virtual floats in TOPAZ (middle) and neXtSIM (right) for the period 2007-2010. The Gaussian (dashed lines) and exponential (dotted lines) fits of the data are also indicated.

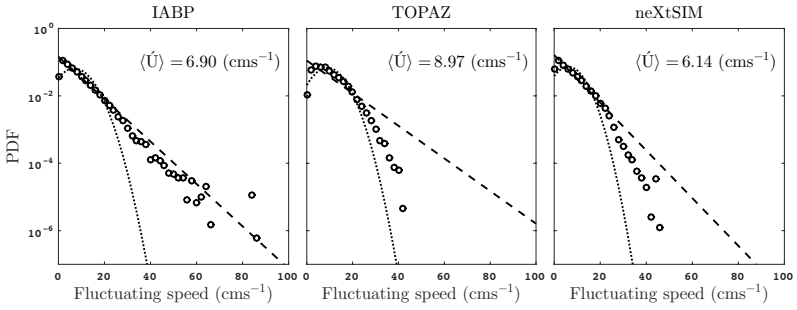

Figure 9. Probability density function of the fluctuating speed of the IABP buoys (left), and of the corresponding virtual floats in TOPAZ (middle) and neXtSIM (right) for the winter periods 2007-2010. The Gaussian (dashed lines) and exponential (dotted lines) fits of the data are also indicated.

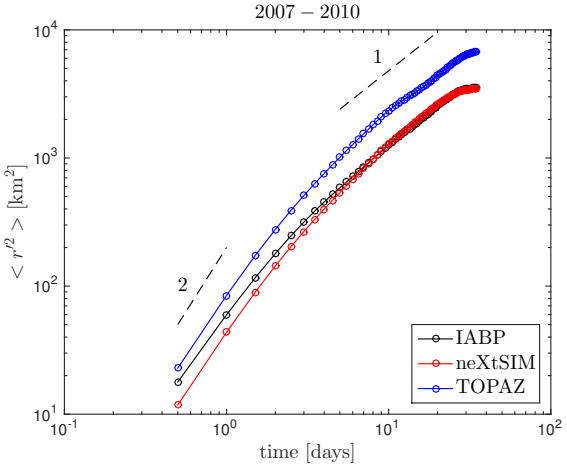

Figure 10. Ensemble mean of the variance of the fluctuating displacement $< r'^2 >$ for the winter seasons 2007-2011 for IABP, TOPAZ and neXtSIM. The dashed lines indicate the theoretical slopes for the two diffusion regimes: the "ballistic" regime ($\langle r'^2(t) \rangle \sim t^2$) which has a slope equal to 2, and the "Brownian" regime ($\langle r'^2(t) \rangle \sim t$) which has a slope equal to 1.

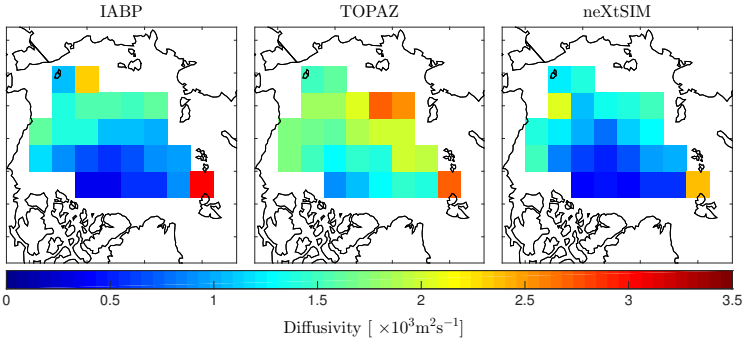

Figure 11. Diffusivity fields obtained from the analysis of the IABP buoys trajectories (left), TOPAZ floats trajectories (middle), and neXtSIM floats trajectories (right) for the winters 2007-2010. The diffusivity is averaged over boxes of 400 by 400 km.

Table 1. This table gives an estimate of the searching radii and areas corresponding to 1, 2 and 3 standard deviations, respectively, and for time horizons ranging from 1 to 30 days. These numbers are averaged over the whole domain and period analysed in Section 2 and should be reevaluated for specific applications, periods and domains of interest, for example by using model outputs having passed the evaluation test proposed in Section 3.

Time horizon [days]	Radius for 1 σ [km]	Area for 1 σ [km^2]	Radius for 2 σ [km]	Area for 2 σ [km^2]	Radius for 3 σ [km]	Area for 3 σ [km^2]
1	10	200	20	900	30	2000
5	30	2600	60	10500	90	23600
10	40	5900	90	23500	130	52900
20	60	11400	120	45400	180	102200
30	70	14900	140	59400	210	133700

Table 2. This table shows the total number of floats (Nrf), the calculated integral time scale (Γ), the variance $\langle u'^2 \rangle$ and the calculated diffusivity K for the different dataset (IABP, TOPAZ and neXtSIM) and time periods used in this study. All these Lagrangian statistics were computed following the diffusion theory of Taylor (1921) and using $L = 400$ km and $T = 165$ days as averaging scales to calculate the Lagrangian mean velocities

$Source$	$Period$	Nrf	$\Gamma(day)$	$\langle u'^2 \rangle (km^2\, day^{-2})$	$K10^3 (m^2 s^{-1})$
IABP	1979-2011	1406	1.4	73	1.2
IABP	2007-2010	280	1.1	64	0.8
TOPAZ	2007-2010	280	1.5	89	1.5
neXtSIM	2007-2010	280	1.3	52	0.8